ACS APPLIED MATERIALS & INTERFACES

Research Article

www.acsami.org

Encapsulating Sn_xSb Nanoparticles in Multichannel Graphene-Carbon Fibers As Flexible Anodes to Store Lithium Ions with High Capacities

Xuan Tang,[†] Feilong Yan,[†] Yuehua Wei,[†] Ming Zhang,[*,†] Taihong Wang,[*,†] and Tianfang Zhang[‡,§]

[†]Key Laboratory for Micro-Nano Optoelectronic Devices of Ministry of Education, School of Physics and Microelectronics, State Key Laboratory for Chemo/Biosensing and Chemometrics, Hunan University, Changsha 410082, China

[‡]Zhuzhou Smelter Group Co. Technology Center, Zhuzhou 412000, China

[§]Hunan Key Laboratory of Lead and Zinc Combined Metallurgy, Zhuzhou 412000, China

ABSTRACT: Sn_xSb intermetallic composites as high theoretical capacities anodes for lithium ion batteries (LIBs) suffer from the quick capacity fading owing to their huge volume change. In this study, flexible mats made up of Sn_xSb-graphene-carbon porous multichannel nanofibers are fabricated by an electrospinning method and succedent annealing treatment at 700 °C. The flexible mats as binder-free anodes show a specific capacity of 729 mA h/g in the 500th cycle at a current density of 0.1 A/g, which is much higher than those of graphene-carbon nanofibers, pure carbon nanofibers, and Sn_xSb-graphene-carbon nanofibers at the same cycle. The flexible mats could provide a reversible capacity of 381 mA h/g at 2 A/g, also higher than those of nanofibers, graphene-carbon nanofibers, and Sn_xSb-carbon nanofibers. It is found that the suitable nanochannels could accommodate the volume expansion to achieve a high specific capacity. Besides, the graphene serves as both conductive and mechanical-property additives to enhance the rate capacity and flexibility of the mats. The electrospinning technique combined with graphene modification may be an effective method to produce flexible electrodes for fuel cells, lithium ion batteries, and super capacitors.

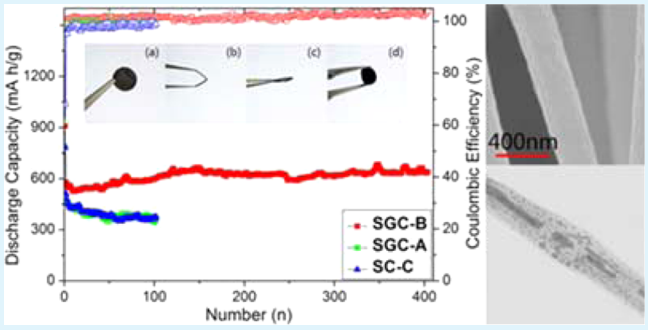

KEYWORDS: *Sn_xSb-graphene-carbon porous multichannel nanofibers, flexible mats, binder free electrodes, good electrical performance, lithium-ion batteries*

INTRODUCTION

A flexible device is of great advantage because of inexpensive production and has been researched by some investigators.[1] It is of great significance to develop flexible devices to satisfy the increasing energy demand of flexible energy-storage equipment.[2] Lithium ion batteries (LIBs) with relatively high power density, inherent high energy density, and eco-friendly property are prospective candidates for energy storage.[3,4] Although the present LIBs are of high properties, the graphite as a typical commercial anode for LIBs are of a theoretical capacity of 372 mA h/g, which is a shortage to improve LIBs properties. Among the candidates for anodes of high-performance LIBs, Li alloy-based anodes have attracted particular attention.[5] According to previous reports, Sn-based anodes with low toxicity and abundant sources have drawn great attention because their theoretical capacities are as high as 990 mA h/g.[6−8] However, with the Li^+ insertion and extraction process, the enormous volume change during the lithiation and delithiation procedure leads to quick fading of reversible capacities, which largely puts off their business application.[9−11] To solve those issues, an alternative method is to prepare Sn-based intermetallic composites (Sn-M), such as $CoSn_3$,[12] Cu_6Sn_5,[13] Ni_3Sn_4,[14] SnSb etc.[15,16] For example, SnSb alloys have been considered the candidates among a variety of Sn-M alloys.[17−22] First, both Sb (660 mA h/g) and Sn (990 mA h/g) can store Li^+ and are conducive to the whole specific capacity. Second, the inert phases could act as buffers to accommodate the volume expansion during the lithiation reaction because the lithiation/delithiation reactions of Sb and Sn occur at different potentials. Therefore, alloying Sn with Sb could reduce the mechanical strain and promote the structural stability as well as the cyclic stability of the anodes.[17,23] Moreover, the lithiation potential of Sb is higher than that of Sn, and the Sn_xSb alloys could be realloyed after the delithiation process.[15,24]

Another possible method to enhance the properties of Sn-M alloys is to provide the space for the volume expansion of Sn-M during lithiation/delithiation procedures. In accordance with previous reports, carbon nanofibers with nanoporosity and hollow channels can promote the electrochemical properties of other anode materials because their flexible, conductive, and

Received: July 17, 2015
Accepted: September 15, 2015
Published: September 15, 2015

DOI: 10.1021/acsami.5b06377
ACS Appl. Mater. Interfaces 2015, 7, 21890−21897

porous structure could accommodate the strain arising from volume changes.[25−29] Whereas, binders would be used to prepare anode electrodes because of the fragility of carbon fiber composites. On the other hand, the binder may block the diffusion of Li^+ and transfer of electrons, resulting in inferior rate capacities.[30] Graphene as a novel 2-D carbon material has outstanding properties, such as high conductivity, excellent stability, and remarkable mechanical property.[31,32] Many articles about graphene-based materials have been published related to energy storage.[33−35] A case in point is that graphene could increase the mechanical property of the nanofibers fabricated by electrospinning.[36,37] Few publications have investigated the preparation of graphene-based materials by electrospinning and corresponding flexible composites as anodes for LIBs. Generally, it is not easy to prepare graphene-based nanofibers with outstanding properties because the dissolvability of graphene in the solvent for electrospinning is so awful, resulting in that the electrospinning with graphene is hard work.

In this work, Sn_xSb-graphene-carbon porous multichannel nanofiber mats (SGC) and Sn_xSb-carbon porous multichannel nanofiber mats (SC) were fabricated by electrospinning and following with an annealing treatment. The graphene oxide for the precursor of electrospinning was processed by an extraordinary way to increase its dispersity in the solvent for the electrospinning procedure. The flexible binder-free mats as anodes for LIBs delivered excellent reversible capacity at a high current density and showed remarkable cyclic stability although the contents of graphene and SnSb alloy particles in final produced nanofibers were very low. The research results demonstrated that the effects of graphene on the properties of the mats included many aspects.

EXPERIMENTAL SECTION

Materials Synthesis. Polyacrylonitrile (PAN, M_W = 150 000, Sigma-Aldrich Co., Ltd.), Poly(methyl methacrylate) (M_W = 35 000, Sinopharm Chemical Reagent Co., Ltd., China), antimony trichloride ($SbCl_3$, Sigma-Aldrich Co., Ltd.), tin(IV) chloride pentahydrate ($SnCl_4{\cdot}5H_2O$, Alfa Aesar Co., Ltd.) and *N*,*N*-dimethylformamide (DMF, Sinopharm Chemical Reagent Co., Ltd., China) were used without any purification. Graphene oxide (GO) was synthesized based on a previous article.[38] The dispersion of GO in DMF was improved by centrifuging and clearing the GO suspension with DMF several times. Then GO with a concentration of approximately 0.4 mg/mL was dispersed in DMF to form a suspension. Next, the suspension was treated using ultrasonic wave for 0.5 h. SGC-A sample was fabricated using 0.478 g of PAN, 0.206 g of PMMA, 0.25 g of $SnCl_4{\cdot}5H_2O$, 0.055 g of $SbCl_3$, and 1 mL of GO dissolved in DMF (the mass ratio of PAN/PMMA is 7:3). The SGC-B sample is 0.342 g of PAN, 0.342 g of PMMA, 0.25 g of $SnCl_4{\cdot}5H_2O$, 0.055 g of $SbCl_3$, and 1 mL of GO dissolved in DMF (the mass ratio of PAN/PMMA is 5:5). The SC-C sample is the same with SGC-B except GO. Finally, all the precursor solution was transferred into a syringe (5 mL) with a stainless steel needle whose inner diameter is 0.6 mm. The flow rate was controlled to be 0.3 mL/h. The distance of an aluminum collector and needle was 12 cm. A high voltage dc power was connected with the needle, and the voltage between the collector and needle was set to be 6−10 kV. Under the conditions, SGC-A, SGC-B, and SC-C were gained and formed the mats. After preoxidized at 230 °C in air for 6 h, the brown mats were annealed at 700 °C in the Ar−H_2 mixture for 2 h to decompose the $SnCl_4$ and $SbCl_3$ and carbonize the PAN and PMMA.

Materials Characterization. The morphology of the samples were observed by a FEI Tecnai G2 F20 transmission electron microscope (TEM) operating at 200 kV accelerating voltage and a Hitachi S4800 scanning electron microscope (SEM). The mats were also analyzed by X-ray photoelectron spectroscopy (XPS). Before the XPS test, the binding energy scales of this equipment were calibrated by assigning the lowest binding energy C 1s peak (a binding energy of 285.0 eV). The thermal gravimetric analysis was recorded on a thermogravimetric analyzer (TGA, PerkinElmer, Diamond TG/DTA) with a heating rate of 3.5 °C/min in air from 30 to 800 °C.

Electrochemical Experiments. The binder-free mats (including SGC-A, SGC-B, and SC-C) were used directly as anodes for LIBs for electrochemical tests. Pure lithium foils severed as both the reference electrodes and the counter electrodes in the batteries. The electrolyte was prepared by dissolving $LiPF_6$ in ethylene carbonate/dimethyl carbonate (the volume ratio is 1:1) to achieve a concentration of 1 M. The separator was Celgard 2400 microporous polypropylene membrane. All the cells (CR 2025) were assembled in a argon-filled glovebox (M. Braun) with the moisture and the oxygen less than 1 ppm. The discharge and charge measurements were carried out by using a Neware and an Arbin BT2000 battery testing system with the cut off potentials being 2.5 V for charge and 0 V for discharge. The specific capacities were calculated based on the weight of the whole mats. The cyclic voltammetry curves were collected on the Arbin BT2000 battery testing system.

RESULTS AND DISCUSSION

Synthesis Method and Characterization of the Mats. Figure 1a−c shows the SEM image of the nanofibers treated at

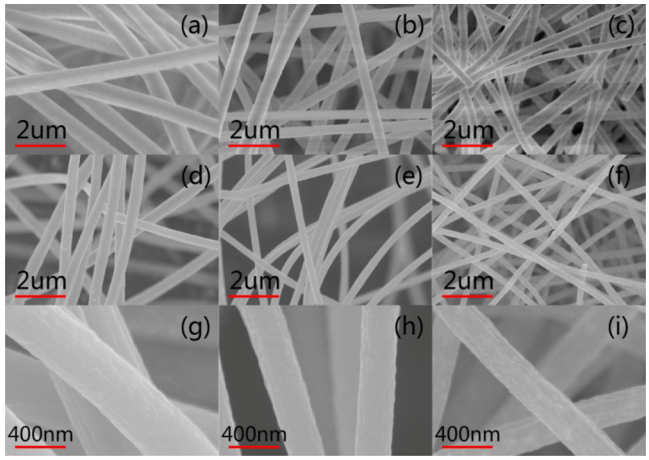

Figure 1. Low-magnification SEM images of SGC-A, SGC-B, and SC-C treated in 230 °C, respectively, parts a−c, and annealed at 700 °C in the H_2/Ar (d−f), and high-magnification of SEM images of SGC-A, SGC-B, and SC-C annealed at 700 °C (g−i).

230 °C. Figure 1d−f shows the low-magnification SEM images of the nanofibers treated at 700 °C. Figure 1g−i shows the high-magnification SEM images of nanofibers treated at 700 °C. The diameter of SGC-A is about 380 nm, while both of SGC-B and SC-C are about 300 nm. Fibers containing the most of PAN are a bit larger than those at similar mass. The graphene oxide was reduced to graphene by thermal treatment in spite of the graphene is not immediately observed in the SEM image.[39] The decrease of the diameters could be attributed to the decomposition of polymers and salts.

Figure 2 shows the flexibility of SGC-B nanofiber mats. The flexible materials (Figure 2a) could bend 60° (Figure 2b) and even 180° (Figure 2c). After the flexibility test, the digital images of nanofiber mats demonstrate that the mats could bend 180° without any mechanical damage (Figure 2d). Figure 2e shows the low-magnification SEM image of the crease line after a bending test. Figure 2f shows the high-magnification SEM image of the crease line after the bending test and the fibers are

DOI: 10.1021/acsami.5b06377
ACS Appl. Mater. Interfaces 2015, 7, 21890−21897

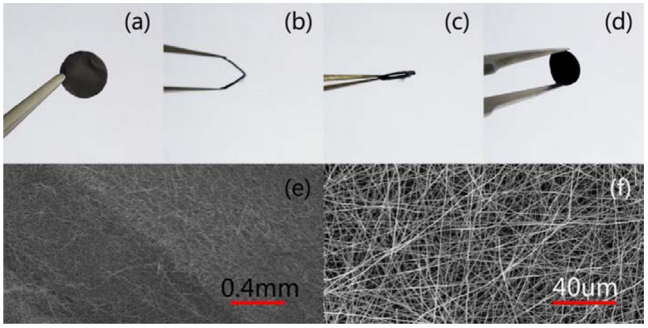

Figure 2. (a–d) Digital photos to show the flexibility of SGC-B nanofiber mats bending 0–60–180–0°. (e,f) SEM images of the crease line after bending tests.

unbroken. That is to say the flexible mats have good mechanical properties.[27,30]

The micromorphology of the fibers was observed using TEM. Figure 3a shows a TEM image of SGC-B. The metal particles inside the porous channel are obvious. The diameters of the nanofibers are about 300 nm.

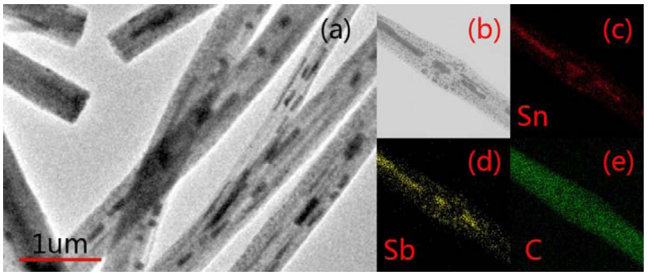

Figure 3. (a) TEM image of SGC-B (b) bright-field TEM image of SGC-B, and (c–e) element mapping images of Sn, Sb, and C, respectively.

For the sake of acquiring the element distribution in the SGC-B nanofibers, a bright-field TEM image and corresponding EDX element maps are displayed in Figure 3b–e. By comparison of the map images of Sn with Sb, it can be concluded that these two elements are mainly dispersed in the channels, which could promote mechanical enhancement and improve conductivity. The carbon map indicates that the position of carbon deposits around the whole SnSb, which demonstrates the Sn_xSb alloy are tidily dispersed in the simultaneously formed successive channel of porous multichannel nanofibers.

The phase purity of SGC-B was characterized by XRD. All the reflection peaks in (Figure 4a) can be assigned to tetragonal α-Sn phase (JCPDS card no. 04-0673) and rhombohedral β-SnSb phase (JCPDS card no. 33-0118). No diffraction peak indexed as graphene was found in the pattern of composites, because most graphene was separated in multichannel nanofibers and the content of graphene in SGC-B was calculated to be 0.079 wt % based on the carbonation rate of 51.8% for PAN/PMMA (5:5) and 70% for GO.[40,41] The HRTEM image (Figure 4b) reveals regular lattice fringes of 0.219 nm, which is in line with the (012) lattice planes of β-SnSb. The HRTEM image (Figure 4c) also shows lattice fringes of 0.30 nm, which is according with the (200) lattice planes of α-Sn phase.

XPS analysis was processed on a Surface Science Instruments S-probe spectrometer to investigate the bond state of SnSb-G-C nanofibers (SGC-B). Figure 5a shows the full XPS spectrum of SGC-B. Figure 5b shows peaks with binding energies 485.15 (metal) and 486.89 eV (Sn–O). The binding energy of 485.15 eV for Sn $3d_{5/2}$ is close to the theoretical value of pure Sn (484.3 eV). No peak at 487.3 eV for SnO_2 appeared, demonstrating that the oxygen atoms are only adsorbed on the surface and there is no atom in a molecular bondage with Sn.[17,42] This is in conformity with the XRD analysis. The binding energy of Sb 3d is close to O 1s (Figure 5c). The signals at 527.8 and 537.3 eV are attributed to antimony metal (XPS value of pure Sb $3d_{3/2}$ at 537.6 eV and Sb $3d_{5/2}$ at 528.2 eV).[43] When carbon is formed at 700°, the carbon surfaces must have unfilled valences and radical sites. Oxygen exists even though a little oxygen will react at these sites. The O 1s can be deconvoluted into three peaks at 530.83, 533.38, and 532.08 eV, which is corresponding to carbonyl oxygen of quinones, noncarbonyl (ether type) oxygen atoms in esters and anhydrides, and carbonyl oxygen atoms in esters.[44,45] Figure 5d shows that there are several nitrogen-containing groups on the multichannel nanofibers, for example pyridinic-N (398.31 eV), pyrrolic-N (400.77 eV), quaternary nitrogen (401.87 eV).[46,47] Generally, the nitrogen functional groups are usually in the following molecular structures. The pyrrolic-N refers to nitrogen atoms bonded to two carbon atoms and contributes to the π system with two p-electrons.[46,47] Pyridinic-N refers to nitrogen atoms at the edge of graphene planes, each of which is bonded to two carbon atoms and donates one p-electron to the aromatic π system.[46,47] Quaternary nitrogen is also called substituted nitrogen or graphitic nitrogen, which are incorporated into graphene layers and replace carbon atoms.[46] All of the above nitrogen have beneficial influence on the storage of Li^+, particularly the pyridine-type nitrogen. Besides, nitrogen

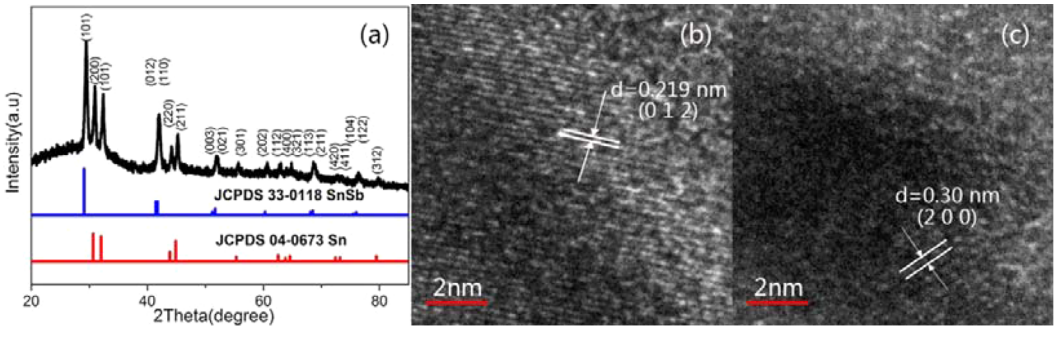

Figure 4. (a) XRD pattern of SGC-B nanofibers and JCPDS date and (b,c) HRTEM images of SGC-B nanofibers.

DOI: 10.1021/acsami.5b06377
ACS Appl. Mater. Interfaces 2015, 7, 21890–21897

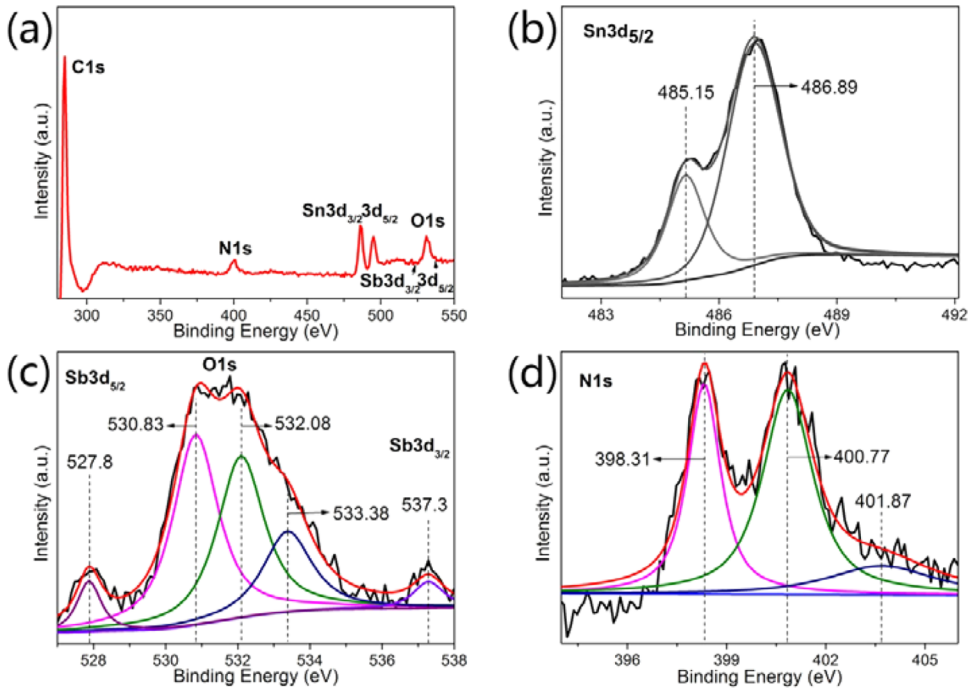

Figure 5. (a) Full XPS spectrum of SGC-B, (b) Sn 3d XPS spectra of SGC-B composite, (c) high resolution Sb 3d and O 1s XPS spectrum of SGC-B, and (d) N 1s XPS spectrum of SGC-B.

doping can promote the conductivity of carbon and generate intensive properties of Li^+ storage.[28]

The molar ratio of $SnCl_4{\cdot}5H_2O$ and $SbCl_3$ in precursors is 3:1 and the heat-treated products are Sb_2O_3 and SnO_2. In accordance with TGA results (Figure 6), the weight ratio of

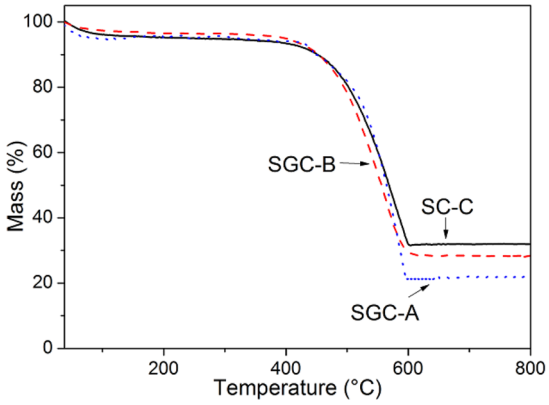

Figure 6. TG curves of SGC-A, SGC-B, and SC-C with a heating rate of 3.5 K/min in air.

Sn/SnSb in the composites could be estimated based on the weight before and after TG tests and the transformation of metal to metal oxide, as described by following equation:

$$\text{Sn/SnSb content (\%)} = 100 \times \frac{\text{molecular weight of } Sn_3Sb}{\text{molecular weight of } Sn_3SbO_{7.5}} \times \frac{\text{final weight}}{\text{initial weight}} \quad (1)$$

the mass ratio of Sn/SnSb in SGC-A, SGC-B, and SC-C is about 18.5%, 22.4%, and 24.5%, respectively, showing that the mass load of Sn/SnSb is very low. The value of SGC-B is similar to SC-C because the content of graphene is very small. The big difference between SGC-A and SGC-B could be attributed to the different carbonation ratio of PAN and PMMA. As previously reported, the PMMA would be burned off nearly so that the residual carbon was almost produced by PAN.[41]

Electrochemical Properties. CV measurements of SGC-B were processed in a voltage range of 0−3 V, and the result is shown in Figure 7a. The cathodic peak of the first cycle at around 0.65 V could be ascribed to forming irreversible solid electrolyte interface (SEI) films.[48] It also can be found that there are two anodic peaks around 0.2 and 1.3 V, which could be attributed to the delithiation of the graphite-like carbon and Li^+ extraction from the defective sites of carbon nanofibers, respectively.[49−51] The CV curves of the followed cycle nearly overlapped, indicating an excellent cyclic stability of SGC-B. A obvious reduction peak at approximately 0.3 V and four oxidation peaks in the range of 0.55−0.89 V are attributed to the multistep lithiation and delithiation reaction of the Li_xSn alloy, which can be observed in both Sn-C and SnSb-C electrodes.[10,24,52] However, a couple of anodic/cathodic peaks locating around 1.17 and 0.76 V (Figure 7a) only can be observed in SnSb, which can be indexed to the reactions between Li and Sb.[18−20,53] Both the delithiation and lithiation voltages of Sb (1.17 and 0.76 V, respectively) are higher than those of Sn, confirming that the SnSb alloys with staged reaction make the volume changes more steady.[10,21] Thus, the reaction of SGC with Li^+ could be described as follows:[54]

$$SnSb + xLi^+ + xe^- \leftrightarrow Li_xSnSb \quad (0 < x < 1.6) \quad (2)$$

$$Li_{1.6}SnSb + 1.4Li^+ + 1.4e^- \leftrightarrow Li_3Sb + Sn \quad (3)$$

$$Sn + 4.4Li^+ + 4.4e^- \leftrightarrow Li_{4.4}Sn \quad (4)$$

$$yC + zLi^+ + ze^- \leftrightarrow Li_zC_y \quad (5)$$

DOI: 10.1021/acsami.5b06377
ACS Appl. Mater. Interfaces 2015, 7, 21890−21897

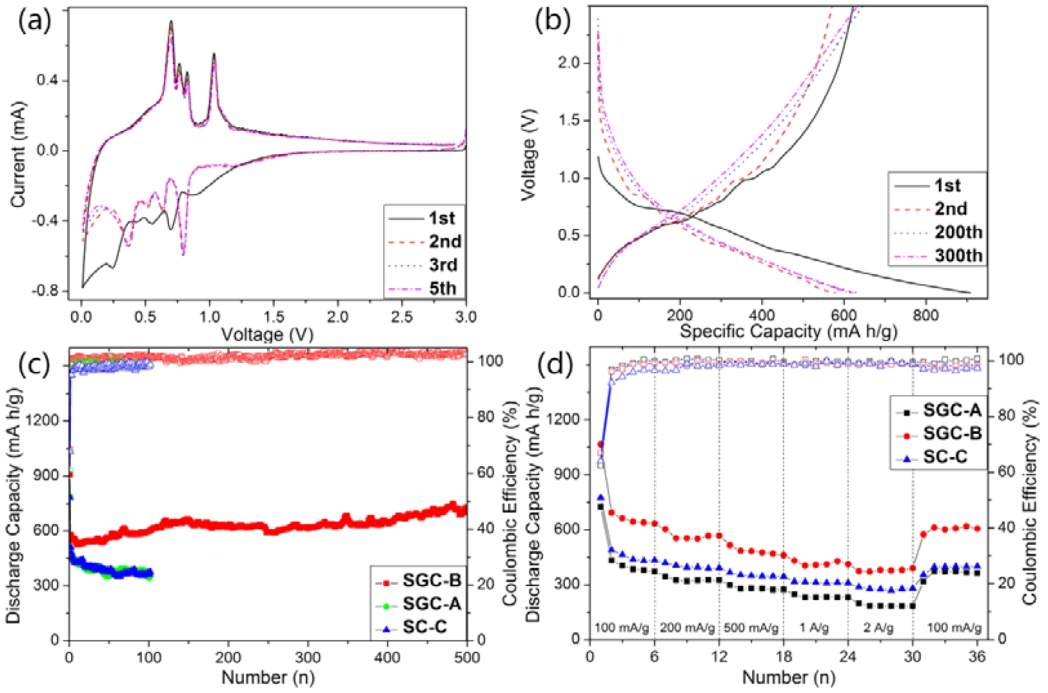

Figure 7. (a) CV curves of SGC-B at a scan rate of 0.3 mV/s. (b) Galvanostatic charge/discharge voltage profiles of SGC-B at a current density of 100 mA/g. (c) Cycling properties and Coulombic efficiency of the samples SGC-A, SGC-B, and SC-C at 100 mA/g. (d) The rate capacities of the samples SGC-A, SGC-B, and SC-C.

Figure 7b shows the discharge−charge curves of SGC-B electrodes in the voltage range of 0−2.5 V at 0.1 A/g. The voltage plateaus of SGC-B are around 1.1 V (charge curve) and 0.8 V (discharge curve), which are matched well with the CV results. The initial lithiation and delithiation capacities of SGC-B were 908 mA h/g and 623 mA h/g, corresponding to an initial Coulombic efficiency of 68%. The reversible capacity of 623 mA h/g is nearly 1.7 times than that of commercial graphite anode (372 mA h/g) although the initial Coulombic efficiency of SGC-B electrode is not so good.[53] Figure 7c compares the discharge capacities of samples (SGC-A, SGC-B, SC-C) as a function of cyclic number at 100 mA/g current densities. SGC-B could provide a discharge capacity of 729 mA h/g after 500 cycles, showing high capacity and super cyclic stability. The discharge capacity of SGC-B (PAN/PMMA = 5:5) is much higher than that of SGC-A (PAN/PMMA = 7:3) after 100 cycles (The capacities are 611 mA h/g and 346 mA h/g, respectively), which could be ascribed to the much higher porosity of the nanofibers which is to the benefit of tolerating the volume expansion of the active materials. Comparing SGC-B with SC-C, it is clear that the discharge capacity of SGC-B is much higher than that of SC-C at a current density of 0.1 A/g (the capacities of SGC-B and SC-C after 100 cycles are 611 mA h/g and 370 mA h/g, respectively), which demonstrates that the synergies among the four compositions (carbon, graphene, Sn, and SnSb) is one of the critical factors in promoting the electrochemical properties of the nanofiber mats. Comparing the properties of SGC-B with previous reports about different Sn/SnSb-based materials, it could be found that SGC-B mats showed a relatively superior cyclic stability and high specific capacity, as displayed in Table 1. Besides, their properties are also better than some of SnSb-C and SnSb-G composites toward the storage of Li^+, indicating the advantages of the flexible SGC-B mats as high property anodes for LIBs. To study the advance of SGC-B mats as electrodes for LIBs, the rate capacities were evaluated, as shown in Figure 7d. The SGC-B keeps reversible capacities of 639, 567, 475, 427, and 381 mA h/g at current densities of 0.1, 0.2, 0.5, 1, 2 A/g, respectively. These values are much higher than those of SGC-A and SC-C at relevant current densities. The enhancement could be ascribed to the improved conductivity by graphene modifying. It should be noticed that the specific capacities of SC-C were higher than those of SGC-A at large current densities while they were almost the same at 100 mA/g. A possible reason was

Table 1. Specific Capacities and Cyclic Properties of SnSb-Carbon Composites As Anodes for LIBs

	capacity (mA h/g)/current density (A/g)			
materials	30th	100th	others	ref
SnSb/G composites	570/0.1	420/0.1		56
porous SnSb/C composites	420/0.1/50th			20
SnSb/carbon nanotube	850/0.1			54
SnSb/G carbon particles	714/0.08			57
SnSb/MgO/C composites	528/0.1	510/0.1	498/0.1 (150th)	24
Sn-Sb-Co alloy	530/0.13	510/0.1	512.8/0.1 (150th)	17
SnSb/C microsphere	564/0.1/60th			58
SnSb/SnO_2/C nanofibers	515/0.05/40th			59
SnSb/C composites	740/0.1	678/0.1	672.2/0.1 (120th)	53
SnSb/C nanoparticles	470/0.05/50th			60
SnSb/C porous nanofibers			646/0.05 (150th)	61
SnSb/G/C mats			729/0.1 (500th)	this study

DOI: 10.1021/acsami.5b06377
ACS Appl. Mater. Interfaces 2015, 7, 21890−21897

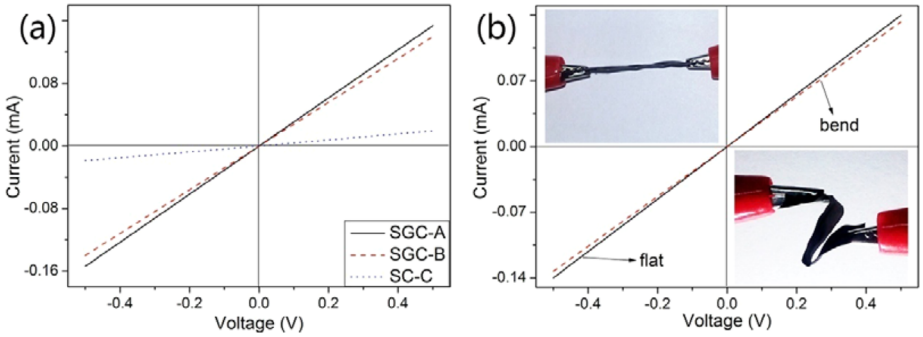

Figure 8. (a) $I-V$ curves of SGC-A, SGC-B, and SC-C and (b) $I-V$ curves of SGC-B for the bending test.

that SC-C with larger porosity for ion diffusion was more beneficial to deliver rate capacities than SGC-A with high conductivity.

The mats were cut into 25 mm × 15 mm and their electrical conductivities were tested by a semiconductor parameter instrument Agilent 4156. The electrical conductivities of SGC and SC mats were measured by a two-probe method.[55] Figure 8a shows the electrical conductivity of each group. The electrical conductivities of SGC-A, SGC-B, and SC-C are 4.20 × 10^{-2}, 3.69 × 10^{-2}, and 6.32 × 10^{-3} S cm^{-1}, respectively. The value of the SGC series is much higher than SC-C, which suggests that although the mass ratio of graphene is negligible on SGC, the impact on electrical conductivity could not be ignored. The electrical conductivity for the bending test is shown on Figure 8b. The digital images show that the flexible mats were bent like an "S" shape. The value of electrical conductivity was similar no matter whether the mats were bent, which demonstrated that the SGC-B mat was a good flexible material for the electrode.

The SEM images of the flexible mats after 50 cycles were shown on Figure 9. The morphology remains of the nanofibers

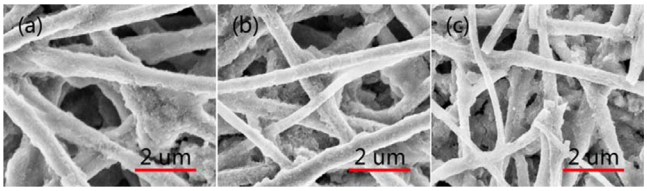

Figure 9. SEM images of SGC-A, SGC-B, and SC-C after 50 cycles, respectively (a–c).

and the diameter of SGC-A remains larger than SGC-B and SC-C. Comparison of Figure 9 with Figure 1, it could be found that the surface of fibers after cycling was rough while the surface before cycling was smooth because of the presence of SEI films. Whichever SGC-A, SGC-B, or SC-C, the morphologies kept well after several cycles, confirming good cyclic stability.

Figure 10a shows the schematic diagram of flexible nanofiber mats. Figure 10b shows a cross-section schematic diagram of nanofibers in the process of deserting the Li^+. Figure 10c shows the cross-section schematic diagram of nanofibers in the process of deserting the Li^+. The compatibility between graphitic carbon and metal particle is so poor, which could account for the precipitation of particles into the channels of nanofibers. The porous multichannel could prevent the metal particle from both pulverization and peeling off.

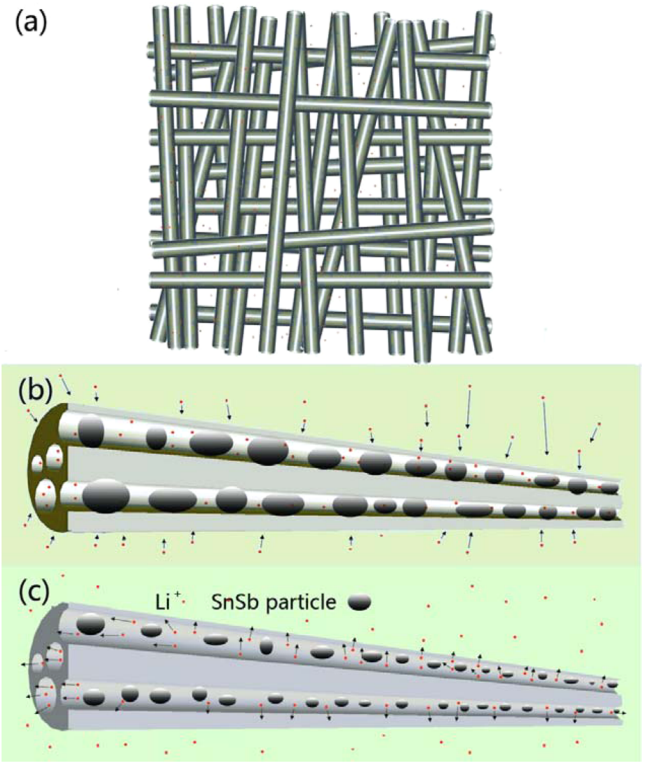

Figure 10. Schematic diagrams: (a) flexible nanofiber mats, (b) cross-section of nanofibers in the process of inserting the Li^+, and (c) cross-section of nanofibers in the process of deserting the Li^+.

CONCLUSIONS

In conclusion, flexible Sn_xSb-graphene-carbon porous multichannel nanofiber mats and flexible Sn_xSb-carbon porous nanofiber mats have been synthesized by an electrospinning method and the following annealing treatment. As binder-free anodes for LIBs, the flexible mats show the good flexibility and the SGC-B displays enhanced cyclic stability as well as high specific capacity (729 mA h/g after 500 cycles at a current density of 0.1 A/g) and enhanced rate capacity (385 mA h/g at a current density of 2 A/g), comparing with SGC-A and SC-C. The outstanding electrochemical properties of SGC-B are mainly attributed to two aspects. First, the graphene reduced from graphene oxide with superior conductivity and excellent mechanical properties could not only improve the conductivity and flexibility of the mats but also decrease the particle diameters of SnO_2 and Sb_2O_3 during the annealing process. Second, the porous multichannel fibers could prevent the metal particle from both pulverization and electrical disconnection

DOI: 10.1021/acsami.5b06377
ACS Appl. Mater. Interfaces 2015, 7, 21890–21897

from the current collector, resulting in excellent cyclic properties.

AUTHOR INFORMATION

Corresponding Authors

*E-mail: zhangming@hnu.edu.cn.
*E-mail: thwang@hnu.edu.cn.

Notes

The authors declare no competing financial interest.

ACKNOWLEDGMENTS

The present work has been supported by the National Natural Science Foundation of China (Grants 51404103, 51574117, 61376073, and 21103046), Fundamental Research Funds for the Central Universities, and the Hunan Provincial Natural Science Foundation of China (Grants 11JJ7004 and 14JJ3067).

REFERENCES

(1) Jia, X.; Chen, Z.; Suwarnasarn, A.; Rice, L.; Wang, X.; Sohn, H.; Zhang, Q.; Wu, B. M.; Wei, F.; Lu, Y. High-Performance Flexible Lithium-Ion Electrodes Based on Robust Network Architecture. *Energy Environ. Sci.* **2012**, *5* (5), 6845−6849.

(2) Kuang, D.; Brillet, J.; Chen, P.; Takata, M.; Uchida, S.; Miura, H.; Sumioka, K.; Zakeeruddin, S. M.; Gratzel, M. Application of Highly Ordered TiO_2 Nanotube Arrays in Flexible Dye-Sensitized Solar Cells. *ACS Nano* **2008**, *2* (6), 1113−1116.

(3) Liu, Y.; Clark, M.; Zhang, Q.; Yu, D.; Liu, D.; Liu, J.; Cao, G. V_2O_5 Nano-Electrodes with High Power and Energy Densities for Thin Film Li-Ion Batteries. *Adv. Energy Mater.* **2011**, *1* (2), 194−202.

(4) Yu, D.; Chen, C.; Xie, S.; Liu, Y.; Park, K.; Zhou, X.; Zhang, Q.; Li, J.; Cao, G. Mesoporous Vanadium Pentoxide Nanofibers with Significantly Enhanced Li-Ion Storage Properties by Electrospinning. *Energy Environ. Sci.* **2011**, *4* (3), 858−861.

(5) Park, C.-M.; Kim, J.-H.; Kim, H.; Sohn, H.-J. Li-Alloy Based Anode Materials for Li Secondary Batteries. *Chem. Soc. Rev.* **2010**, *39* (8), 3115−3141.

(6) Zhou, X.; Dai, Z.; Liu, S.; Bao, J.; Guo, Y. G. Ultra-Uniform SnO_x/Carbon Nanohybrids toward Advanced Lithium-Ion Battery Anodes. *Adv. Mater.* **2014**, *26* (23), 3943−3949.

(7) Winter, M.; Besenhard, J. O. Electrochemical Lithiation of Tin and Tin-Based Intermetallics and Composites. *Electrochim. Acta* **1999**, *45* (1), 31−50.

(8) Chen, J. S.; Lou, X. W. D. SnO_2-Based Nanomaterials: Synthesis and Application in Lithium-Ion Batteries. *Small* **2013**, *9* (11), 1877−1893.

(9) Zhou, X.; Zou, Y.; Yang, J. Periodic Structures of Sn Self-Inserted between Graphene Interlayers as Anodes for Li-Ion Battery. *J. Power Sources* **2014**, *253*, 287−293.

(10) Chao, S.-C.; Song, Y.-F.; Wang, C.-C.; Sheu, H.-S.; Wu, H.-C.; Wu, N.-L. Study on Microstructural Deformation of Working Sn and SnSb Anode Particles for Li-Ion Batteries by in Situ Transmission X-Ray Microscopy. *J. Phys. Chem. C* **2011**, *115* (44), 22040−22047.

(11) Sun, X.; Wang, X.; Qiao, L.; Hu, D.; Feng, N.; Li, X.; Liu, Y.; He, D. Electrochemical Behaviors of Porous SnO_2-Sn/C Composites Derived from Pyrolysis of SnO_2/Poly (vinylidene fluoride). *Electrochim. Acta* **2012**, *66*, 204−209.

(12) Gu, Y.; Wu, F.; Wang, Y. Confined Volume Change in Sn-Co-C Ternary Tube-in-Tube Composites for High-Capacity and Long-Life Lithium Storage. *Adv. Funct. Mater.* **2013**, *23* (7), 893−899.

(13) Chen, J.; Yang, L.; Fang, S.; Zhang, Z.; Hirano, S.-i. Facile Fabrication of Graphene/Cu_6Sn_5 Nanocomposite as the High Performance Anode Material for Lithium-Ion Batteries. *Electrochim. Acta* **2013**, *105*, 629−634.

(14) Gowda, S. R.; Reddy, A. L. M.; Shaijumon, M. M.; Zhan, X.; Ci, L.; Ajayan, P. M. Conformal Coating of Thin Polymer Electrolyte Layer on Nanostructured Electrode Materials for Three-Dimensional Battery Applications. *Nano Lett.* **2011**, *11* (1), 101−106.

(15) Li, H.; Wang, Q.; Shi, L.; Chen, L.; Huang, X. Nanosized SnSb Alloy Pinning on Hard Non-Graphitic Carbon Spherules as Anode Materials for a Lithium-Ion Battery. *Chem. Mater.* **2002**, *14* (1), 103−108.

(16) Park, M.-S.; Needham, S. A.; Wang, G.-X.; Kang, Y.-M.; Park, J.-S.; Dou, S.-X.; Liu, H.-K. Nanostructured SnSb/Carbon Nanotube Composites Synthesized by Reductive Precipitation for Lithium-Ion Batteries. *Chem. Mater.* **2007**, *19* (10), 2406−2410.

(17) Ke, F.-S.; Huang, L.; Solomon, B. C.; Wei, G.-Z.; Xue, L.-J.; Zhang, B.; Li, J.-T.; Zhou, X.-D.; Sun, S.-G. Three-Dimensional Nanoarchitecture of Sn-Sb-Co Alloy as an Anode of Lithium-Ion Batteries with Excellent Lithium Storage Performance. *J. Mater. Chem.* **2012**, *22* (34), 17511−17517.

(18) Li, J.; Ru, Q.; Hu, S.; Sun, D.; Zhang, B.; Hou, X. Spherical Nano-SnSb/MCMB/Carbon Core-Shell Composite for High Stability Lithium-Ion Battery Anodes. *Electrochim. Acta* **2013**, *113*, 505−513.

(19) Li, X.; He, X.; Xu, Y.; Huang, L.; Li, J.; Sun, S.; Zhao, J. Superiority of the Bi-Phasic Mixture of a Tin-Based Alloy Nanocomposite as the Anode for Lithium-Ion Batteries. *J. Mater. Chem. A* **2015**, *3* (7), 3794−3800.

(20) Park, C.-M.; Jeon, K.-J. Porous Structured SnSb/C Nanocomposites for Li-Ion Battery Anodes. *Chem. Commun.* **2011**, *47* (7), 2122−2124.

(21) Park, C.-M.; Sohn, H.-J. A Mechano-and Electrochemically Controlled SnSb/C Nanocomposite for Rechargeable Li-Ion Batteries. *Electrochim. Acta* **2009**, *54* (26), 6367−6373.

(22) Zhou, X.; Dai, Z.; Bao, J.; Guo, Y.-G. Wet Milled Synthesis of an Sb/MWCNT Nanocomposite for Improved Sodium Storage. *J. Mater. Chem. A* **2013**, *1* (44), 13727−13731.

(23) Zhao, H.; Yin, C.; Guo, H.; He, J.; Qiu, W.; Li, Y. Studies of the Electrochemical Performance of Sn-Sb Alloy Prepared by Solid-State Reduction. *J. Power Sources* **2007**, *174* (2), 916−920.

(24) Seo, J.-U.; Park, C.-M. Nanostructured SnSb/MO_x (M= Al or Mg)/C Composites: Hybrid Mechanochemical Synthesis and Excellent Li Storage Performances. *J. Mater. Chem. A* **2013**, *1* (48), 15316−15322.

(25) Zhou, X.; Wan, L. J.; Guo, Y. G. Electrospun Silicon Nanoparticle/Porous Carbon Hybrid Nanofibers for Lithium-Ion Batteries. *Small* **2013**, *9* (16), 2684−2688.

(26) Ji, L.; Rao, M.; Aloni, S.; Wang, L.; Cairns, E. J.; Zhang, Y. Porous Carbon Nanofiber-Sulfur Composite Electrodes for Lithium/Sulfur Cells. *Energy Environ. Sci.* **2011**, *4* (12), 5053−5059.

(27) Kim, C.; Jeong, Y. I.; Ngoc, B. T. N.; Yang, K. S.; Kojima, M.; Kim, Y. A.; Endo, M.; Lee, J. W. Synthesis and Characterization of Porous Carbon Nanofibers with Hollow Cores through the Thermal Treatment of Electrospun Copolymeric Nanofiber Webs. *Small* **2007**, *3* (1), 91−95.

(28) Su, Y.-S.; Manthiram, A. Lithium-Sulphur Batteries with a Microporous Carbon Paper as a Bifunctional Interlayer. *Nat. Commun.* **2012**, *3*, 1166−1171.

(29) Ji, L.; Gu, M.; Shao, Y.; Li, X.; Engelhard, M. H.; Arey, B. W.; Wang, W.; Nie, Z.; Xiao, J.; Wang, C. Controlling SEI Formation on SnSb-Porous Carbon Nanofibers for Improved Na-Ion Storage. *Adv. Mater.* **2014**, *26* (18), 2901−2908.

(30) Zhang, M.; Yan, F.; Tang, X.; Li, Q.; Wang, T.; Cao, G. Flexible CoO-Graphene-Carbon Nanofiber Mats as Binder-Free Anodes for Lithium-Ion Batteries with Superior Rate Capacity and Cyclic Stability. *J. Mater. Chem. A* **2014**, *2* (16), 5890−5897.

(31) Allen, M. J.; Tung, V. C.; Kaner, R. B. Honeycomb Carbon: a Review of Graphene. *Chem. Rev.* **2010**, *110* (1), 132−145.

(32) Ding, S.; Luan, D.; Boey, F. Y. C.; Chen, J. S.; Lou, X. W. D. SnO_2 Nanosheets Grown on Graphene Sheets with Enhanced Lithium Storage Properties. *Chem. Commun.* **2011**, *47* (25), 7155−7157.

(33) Kim, C. H.; Kim, B.-H.; Yang, K. S. TiO_2 Nanoparticles Loaded on Graphene/Carbon Composite Nanofibers by Electrospinning for Increased Photocatalysis. *Carbon* **2012**, *50* (7), 2472−2481.

(34) Liang, J.; Jiao, Y.; Jaroniec, M.; Qiao, S. Z. Sulfur and Nitrogen Dual-Doped Mesoporous Graphene Electrocatalyst for Oxygen

DOI: 10.1021/acsami.5b06377
ACS Appl. Mater. Interfaces 2015, 7, 21890−21897

Reduction with Synergistically Enhanced Performance. *Angew. Chem., Int. Ed.* **2012**, *51* (46), 11496−11500.
(35) Tai, Z.; Yan, X.; Lang, J.; Xue, Q. Enhancement of Capacitance Performance of Flexible Carbon Nanofiber Paper by Adding Graphene Nanosheets. *J. Power Sources* **2012**, *199*, 373−378.
(36) He, Y.; Zhang, N.; Gong, Q.; Qiu, H.; Wang, W.; Liu, Y.; Gao, J. Alginate/Graphene Oxide Fibers with Enhanced Mechanical Strength Prepared by Wet Spinning. *Carbohydr. Polym.* **2012**, *88* (3), 1100−1108.
(37) Zhou, X.; Liu, X.; Xu, Y.; Liu, Y.; Dai, Z.; Bao, J. An SbO_x/Reduced Graphene Oxide Composite as a High-Rate Anode Material for Sodium-Ion Batteries. *J. Phys. Chem. C* **2014**, *118* (41), 23527−23534.
(38) Offeman, R.; Hummers, W. Preparation of Graphitic Oxide. *J. Am. Chem. Soc.* **1958**, *80*, 1339−1339.
(39) Wu, Z.-S.; Ren, W.; Gao, L.; Zhao, J.; Chen, Z.; Liu, B.; Tang, D.; Yu, B.; Jiang, C.; Cheng, H.-M. Synthesis of Graphene Sheets with High Electrical Conductivity and Good Thermal Stability by Hydrogen Arc Discharge Exfoliation. *ACS Nano* **2009**, *3* (2), 411−417.
(40) Niu, Z.; Chen, J.; Hng, H. H.; Ma, J.; Chen, X. A Leavening Strategy to Prepare Reduced Graphene Oxide Foams. *Adv. Mater.* **2012**, *24* (30), 4144−4150.
(41) Zhang, L.; Hsieh, Y.-L. Carbon Nanofibers with Nanoporosity and Hollow Channels from Binary Polyacrylonitrile Systems. *Eur. Polym. J.* **2009**, *45* (1), 47−56.
(42) Cox, D. F.; Fryberger, T. B.; Semancik, S. Surface Reconstructions of Oxygen Deficient SnO_2 (110). *Surf. Sci.* **1989**, *224* (1), 121−142.
(43) Balan, L.; Schneider, R.; Billaud, D.; Lambert, J.; Ghanbaja, J. A Novel Solution-Phase and Low-Temperature Synthesis of SnSb Nano-Alloys. *Mater. Lett.* **2005**, *59* (23), 2898−2902.
(44) Lakshminarayanan, P. V.; Toghiani, H.; Pittman, C. U. Nitric Acid Oxidation of Vapor Grown Carbon Nanofibers. *Carbon* **2004**, *42* (12), 2433−2442.
(45) Lee, S. H.; Mathews, M.; Toghiani, H.; Wipf, D. O.; Pittman, C. U., Jr. Fabrication of Carbon-Encapsulated Mono-And Bimetallic (Sn and Sn/Sb Alloy) Nanorods. Potential Lithium-Ion Battery Anode Materials. *Chem. Mater.* **2009**, *21* (11), 2306−2314.
(46) Arrigo, R.; Hävecker, M.; Schlögl, R.; Su, D. S. Dynamic Surface Rearrangement and Thermal Stability of Nitrogen Functional Groups on Carbon Nanotubes. *Chem. Commun.* **2008**, *40*, 4891−4893.
(47) Matter, P. H.; Zhang, L.; Ozkan, U. S. The Role of Nanostructure in Nitrogen-Containing Carbon Catalysts for the Oxygen Reduction Reaction. *J. Catal.* **2006**, *239* (1), 83−96.
(48) Xiao, L.; Cao, Y.; Xiao, J.; Wang, W.; Kovarik, L.; Nie, Z.; Liu, J. High Capacity, Reversible Alloying Reactions in SnSb/C Nanocomposites for Na-Ion Battery Applications. *Chem. Commun.* **2012**, *48* (27), 3321−3323.
(49) Guo, B.; Wang, X.; Fulvio, P. F.; Chi, M.; Mahurin, S. M.; Sun, X. G.; Dai, S. Soft-Templated Mesoporous Carbon-Carbon Nanotube Composites for High Performance Lithium-Ion Batteries. *Adv. Mater.* **2011**, *23* (40), 4661−4666.
(50) Takami, N.; Satoh, A.; Oguchi, M.; Sasaki, H.; Ohsaki, T. 7 Li NMR and ESR Analysis of Lithium Storage in a High-Capacity Perylene-Based Disordered Carbon. *J. Power Sources* **1997**, *68* (2), 283−286.
(51) Wu, Y.-P.; Wan, C.-R.; Jiang, C.-Y.; Fang, S.-B.; Jiang, Y.-Y. Mechanism of Lithium Storage in Low Temperature Carbon. *Carbon* **1999**, *37* (12), 1901−1908.
(52) Rosenwald, A.; Wright, G.; Chan, W. C.; Connors, J. M.; Campo, E.; Fisher, R. I.; Gascoyne, R. D.; Muller-Hermelink, H. K.; Smeland, E. B.; Giltnane, J. M. The Use of Molecular Profiling to Predict Survival after Chemotherapy for Diffuse Large-B-Cell Lymphoma. *N. Engl. J. Med.* **2002**, *346* (25), 1937−1947.
(53) Fan, L.; Zhang, J.; Zhu, Y.; Zhu, X.; Liang, J.; Wang, L.; Qian, Y. Comparison between SnSb-C and Sn-C Composites as Anode Materials for Lithium-Ion Batteries. *RSC Adv.* **2014**, *4* (107), 62301−62307.
(54) Fan, S.; Sun, T.; Rui, X.; Yan, Q.; Hng, H. H. Cooperative Enhancement of Capacities in Nanostructured SnSb/Carbon Nanotube Network Nanocomposite as Anode for Lithium-Ion Batteries. *J. Power Sources* **2012**, *201*, 288−293.
(55) Chen, Z.; Ren, W.; Gao, L.; Liu, B.; Pei, S.; Cheng, H.-M. Three-Dimensional Flexible and Conductive Iinterconnected Graphene Networks Grown by Chemical Vapour Deposition. *Nat. Mater.* **2011**, *10* (6), 424−428.
(56) Seng, K. H.; Guo, Z. P.; Chen, Z. X.; Liu, H. K. SnSb/Graphene Composite as Anode Materials for Lithium-Ion Batteries. *Adv. Sci. Lett.* **2011**, *4* (1), 18−23.
(57) Chen, S.; Chen, P.; Wu, M.; Pan, D.; Wang, Y. Graphene Supported Sn-Sb@ Carbon Core-Shell Particles as a Superior Anode for Lithium-Ion Batteries. *Electrochem. Commun.* **2010**, *12* (10), 1302−1306.
(58) Wang, K.; He, X.; Ren, J.; Wang, L.; Jiang, C.; Wan, C. Preparation of Sn_2Sb Alloy Encapsulated Carbon Microsphere Anode Materials for Li-Ion Batteries by Carbothermal Reduction of the Oxides. *Electrochim. Acta* **2006**, *52* (3), 1221−1225.
(59) Kim, J.-C.; Kim, D.-W. Synthesis of Multiphase SnSb Nanoparticles-on-SnO_2/Sn/C Nanofibers for Use in Li and Na Ion Battery Electrodes. *Electrochem. Commun.* **2014**, *46*, 124−127.
(60) Niu, X.; Zhou, H.; Li, Z.; Shan, X.; Xia, X. Carbon-Coated SnSb Nanoparticles Dispersed in Reticular Structured Nanofibers for Lithium-Ion Battery Anodes. *J. Alloys Compd.* **2015**, *620*, 308−314.
(61) Xue, L.; Xia, X.; Tucker, T.; Fu, K.; Zhang, S.; Li, S.; Zhang, X. A Simple Method to Encapsulate SnSb Nanoparticles into Hollow Carbon Nanofibers with Superior Lithium-Ion Storage Capability. *J. Mater. Chem. A* **2013**, *1* (44), 13807−13813.

DOI: 10.1021/acsami.5b06377
ACS Appl. Mater. Interfaces 2015, 7, 21890−21897